

A kinematic comparisons of conventional processing, DMO-PSI, and EOM

John C. Bancroft, Gary F. Margrave, and Hugh D. Geiger

ABSTRACT

It has been suggested that equivalent offset migration (EOM) is identical to Gardner's DMO-PSI. This paper is intended to clarify the differences between the two methods by comparing the kinematics of each method. In addition, a comparison with the conventional processing methods of NMO, NMO and DMO, and NMO, DMO, and poststack migration, is included.

BASIC MODELS

Summation and distribution models

Kirchhoff migration sums energy along "diffractions" and places the summed energy at the output location of a migrated sample; usually at the apex of the diffraction. In contrast, a constant velocity *distribution* algorithm will take one input sample and spread its energy along a semicircle. In a constant velocity and infinite aperture environment, both algorithms produce the same result and will produce the typical migration smiles from input noise.

The same principles apply to modelling where an input geological model is used to create a synthetic seismic section. Energy may be summed along semicircles and placed at the bottom of the semicircle, or energy from input samples could be distributed on diffractions.

The RMS assumption

One of the most important advances in seismic processing was the concept of RMS velocities and the resulting simplification that allows linear raypaths to be an approximation to the true (nonlinear) raypaths (Dix 1955), as illustrated in Figure 1. This assumption is the basis of NMO removal and Kirchhoff time migrations. It allows time and offset to be related by Pythagoras's theorem, giving the hyperbolic equation

$$T^2 = T_0^2 + \frac{h^2}{V^2}, \quad (1)$$

where T is the one-way traveltime, T_0 the vertical one-way traveltime, h the half source-receiver offset, and V the RMS velocity defined by Tanner and Koehler (1969). This equation, using the RMS velocities, strictly applies for small offsets, however, seismic reflections tend to be hyperbolic over a much larger range of offset. When stacking dipping data, equation (1) may be changed to include a dip term.

Moveout is still hyperbolic, but in practice the dip effect is included in the velocity, which is then referred to as the stacking velocity.

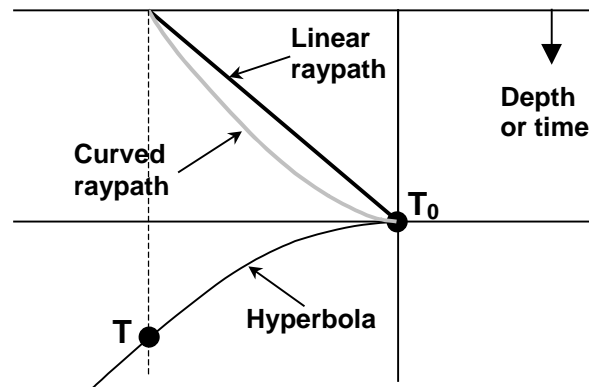


Figure 1 Simplification of curved raypath to linear raypath using RMS velocities.

Scatterpoint model

A simple model used to compare the various methods is shown in Figure 2. This 2-D figure shows an input seismic trace with source S and receiver R that contains energy from a scatterpoint. The trace is located at the common midpoint (CMP) between the source and receiver.

All raypaths to and from the scatterpoint are assumed to be linear with the *velocity* defined at the scatterpoint. We loosely use the term “RMS velocity” to represent that velocity which best satisfies the hyperbolic assumption of rays traveling between a reflection point and the surface. In addition, we will simply use the term “NMO” when referring to NMO removal. When applying the NMO kinematic correction for Kirchhoff migration we use the term “Kirchhoff NMO” which includes the appropriate phase filtering, antialiasing filtering, and scaling.

The RMS assumption is one that will eventually be replaced by “true raypath” estimations of prestack depth migration. However it is still required for verifying acquisition geometry and estimating statics. Its use in prestack time migration leads to a much faster and more economical product than a prestack depth migration. The time algorithms may be used by a seismic processor with little knowledge of the geological structure, and often provides a solution where other methods fail.

Traditionally, the source and receiver rays are ignored in favor of the common midpoint (CMP) concept that was originally designed for specular horizontal reflectors. Consequently, conventional velocity analysis is still based on the half source-receiver offset h . A scatter point approach that considered the dimensions of the actual raypath such as the distances $x + h$ and $x - h$ might provide a more accurate estimation of the velocity.

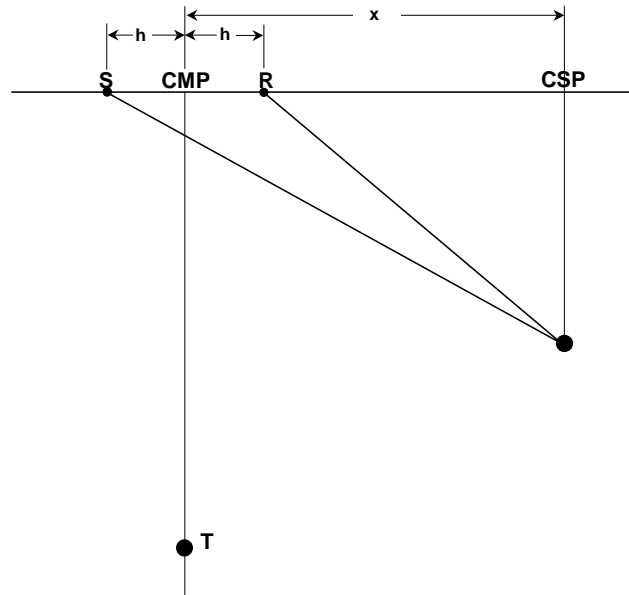


Figure 2 Geometry for a reflection from a dipping event.

Double square root equation

The total traveltime T from a source to a scatterpoint and from a scatterpoint to a receiver is defined by the traveltime of the individual (and linear) raypaths. Each raypath is defined using the RMS velocity and the NMO equation (1) giving,

$$T = \left(T_0^2 + \frac{(x+h)^2}{V^2} \right)^{1/2} + \left(T_0^2 + \frac{(x-h)^2}{V^2} \right)^{1/2} \quad (2)$$

where x defines the horizontal distance from the CMP location to the scatterpoint, h the half source-receiver distance, and T_0 the vertical traveltime from the scatterpoint to the surface.

Cheop's pyramid

If the reflector in Figure 2 is a scatterpoint, then the reflections of a continuum of source and receiver locations may be plotted in a prestack volume (x, h, t) . A surface formed from these reflections is referred to as Cheop's pyramid and is shown in Figure 3.

The objective of seismic imaging is to gather the energy from a scatterpoint and place it back at the original reflector position. The objective, relative to Figure 3, is to sum all the energy distributed over Cheop's pyramid and place it back at the scatterpoint.

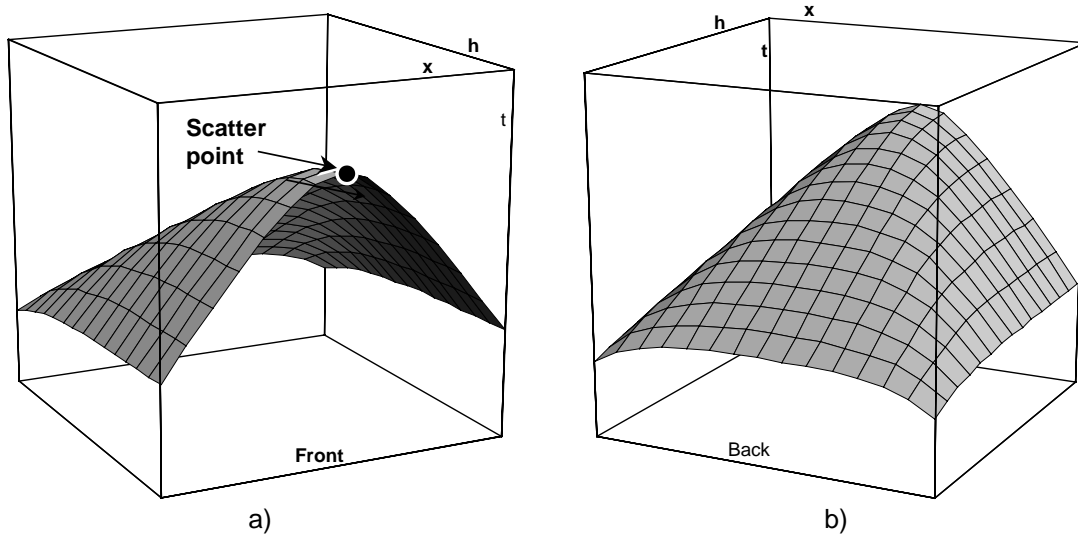


Figure 3. The surface of Cheop's pyramid formed by the reflection times of a scatterpoint. The surface assumes a continuum of many source and receivers.

Input sample and the prestack migration ellipse

An alternate view of prestack migration is to view the distribution of energy from one input sample. This vantage point offers a different perspective and is often associated with Green's functions or an impulse response.

We define the input sample to be located at the *origin* ($x = 0$) with the source and receiver located at $\pm h$, and with scatterpoints located at the spatial position x . In a constant velocity environment, all scatterpoints having the same time T are located on the prestack migration ellipse shown in Figure 4.

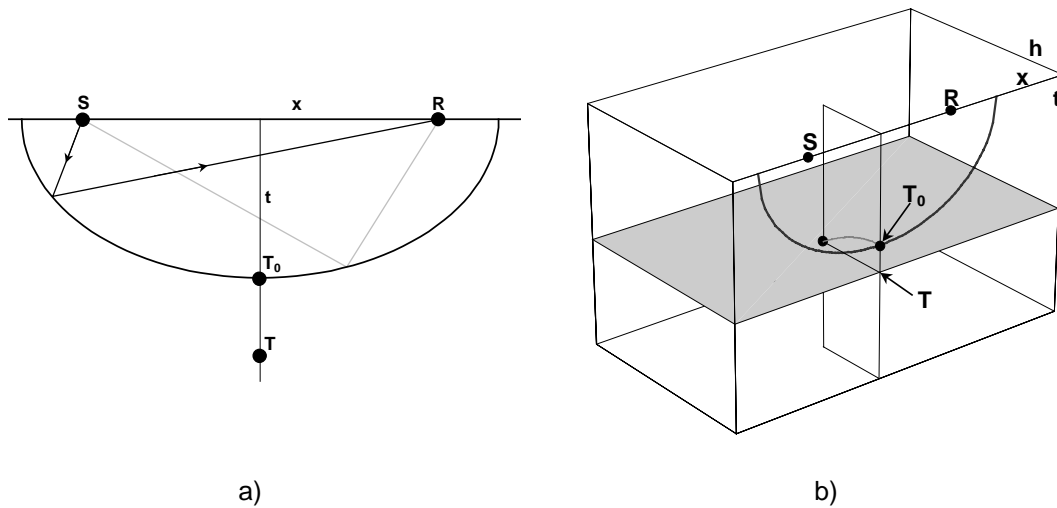


Figure 4 The prestack migration ellipse in a) a constant offset section, b) the prestack volume.

The RMS assumption favors the summation approach for migrating real data as it is based on one scatter point where all raypaths have the same velocity. With the distribution approach, an input sample is distributed to many scatterpoints, each with different velocities. Consequently, the distribution model is more restrictive than the scatterpoint model, but does offer an additional perspective and unique insights.

CONVENTIONAL PROCESSING METHODS

NMO processing

Conventional processing that removes normal moveout (NMO) is based on the assumption of horizontal reflectors. The resulting common midpoint gathers (CMP's) contain all the reflection information. When dipping events are present, the stacking velocity V_{stk} is increased by dividing the horizontal velocity V by the cosine of the dip β , i.e.

$$V_{stk} = \frac{V}{\cos \beta} \quad (3)$$

Use of V_{stk} allows dipping events to stack coherently, however, the reflection points were smeared along the dip causing a loss of resolution. This weakness in the method may be visualized by examining the CMP gathers on the flanks of Cheop's pyramid in Figure 2, where the shape of the scattered energy is non-hyperbolic. The curvature at zero offset however, matches the curvature of a hyperbola with velocities V_{stk} . The larger offset will deviate from the hyperbolic path forming an incomplete image.

The result, even for constant velocities:

- Dipping events smear the energy along the dip.
- Diffractions don't stack.
- Two separate velocity functions required: NMO and poststack migration.

NMO and DMO processing

The inclusion of dip moveout (DMO) processing for a constant velocity eliminates the requirement that stacking velocities for dipping events be increased (equation (3)). The NMO velocity would be the same everywhere, and the subsequent DMO would reshape the energy at all offsets to be identical to zero offset as illustrated in Figure 3. This figure shows the result of applying NMO at constant velocity in (a), with the DMO'd result in (b). All offsets in (b) contain the same shape, and stacking will produce a coherent hyperbola.

DMO may be applied to source records or constant offset sections, and when stacked, should produce identical results. This is the case when the velocities are known exactly. When the velocity (still constant) is unknown, the data may be NMO'd with the incorrect velocity V_j , DMO'd, and then inverse NMO'd (INMO) with same velocity V_j . The INMO must assume some offset for the input traces, which is usually the offset defined by the source gather or constant offset section. A

subsequent velocity analysis attempts to estimate the correct stacking velocity, however, a number of iterations may be required to converge on the desired velocity.

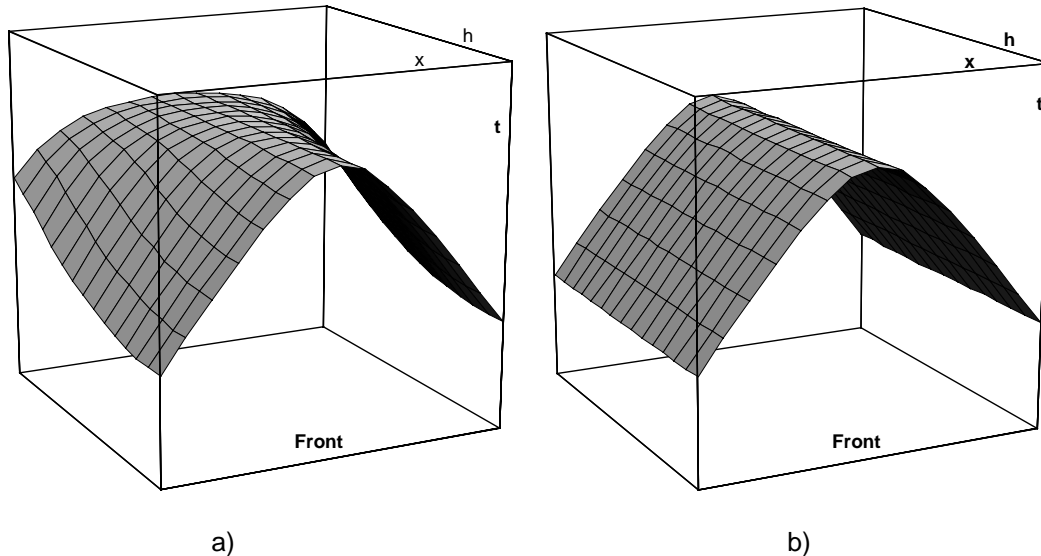


Figure 5 Prestack volumes of a) Cheep's pyramid with NMO results, and b) when followed by DMO produces b).

The NMO-DMO-INMO process is illustrated in Figure 6 which shows the kinematic steps for a sample at time $T = 5$ with half source-receiver offset $h = \pm 3$. After NMO with the correct velocity, the sample is shifted to time $T_{nmo} = 4$. Figure (a) shows DMO using the correct NMO velocity. The thin portion of the curve shows the entire ellipse, with the thicker portion showing the location of DMO'd energy (confined to dips less than 45 degrees). In the subsequent figures, this correct DMO is shown in gray. Figure (b) shows the DMO'd result when using a NMO velocity 30 percent too low which moves the NMO'd time to approximately 2.6. Using the initial velocity, INMO of the DMO curve in (b) is shown in black in Figure (c) where the bottom the ellipse is once again at time T . Velocity analysis may yield the correct velocity for NMO. Application of NMO using the correct velocity is shown in (d) where we observe the zero displacement time is correct at 4.0. However the remaining portion of the curve is displaced from the correct solution shown in gray. These figures illustrate the need to recompute DMO once an accurate velocity is established.

The results of Figure 6 illustrate that a number of iterations may be required to converge to the correct velocity. The shallower dipping events will converge first with the steeper events requiring more iterations. It should also be evident, that when an improved velocity is estimated, the processing should start with the original data requiring DMO to be performed again.

The requirement of constant velocities for DMO may be relaxed to allow processing of data with smoothly varying velocities. Appropriate data includes some marine or stratigraphic plays where the velocities vary smoothly in both horizontal

and vertical directions. In other areas the velocities may vary too rapidly and DMO may actually harm the data.

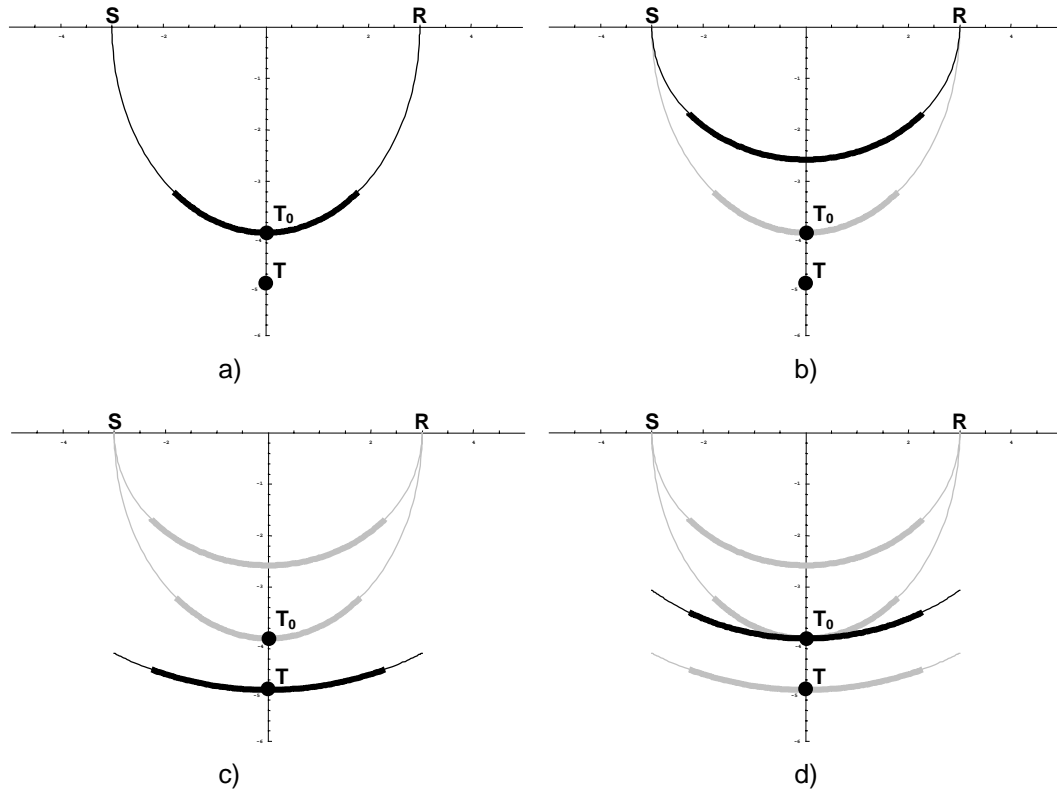


Figure 6 Sequential processes showing a) the correct DMO, b) NMO and DMO with velocities 30 percent too low, c) the subsequent INMO, and d) the resulting NMO with the correct velocities.

The velocity of diffraction energy is defined at the scatterpoint location, however, the energy will appear later in time and overlap deeper events with different velocities. DMO is unable to resolve these velocity conflicts in CMP gathers.

NMO and DMO that uses stacking velocities from previous processing will have large velocity errors in portions of the data with dipping events. Areas with geological dips at 45 degrees will have a stacking velocity increased by 30 percent.

There are some DMO algorithms that are designed for variable velocities but their implementations are rare, and will not be discussed in this paper.

The results using DMO with constant velocities:

- Smear of dipping events is eliminated.
- Diffractions stack.
- Stacking velocities are independent of dip.
- A number of iterations may be required to converge to the correct velocity.
- Two separate velocity functions required: NMO and poststack migration.

The results using DMO with smoothly varying velocities:

- Stacking velocities are independent of dip.
- Multiple velocity solutions will remain in areas of conflicting dip.
- Two separate velocity functions required: NMO and poststack migration.

NMO, DMO, and poststack migration before INMO

The previous discussion where NMO-DMO-INMO is followed by velocity analysis highlighted problems with velocities from conflicting dips. These problems are resolved by including poststack migration of constant offset sections before the INMO step. This process is often referred to as prestack migration and is typically applied to constant offset sections. The migration step tends to position the data in the correct spatial location, which, after INMO, minimizes the problems of conflicting dips. When the correct velocities for NMO and poststack migration are used, the result is a reconstruction of the prestack migration ellipse.

Figure 7 illustrates the process of NMO, DMO, migration, and INMO when an incorrect velocity is used. The prestack migration ellipse in Figure 7a is produced using the correct velocity. Figure 7b shows the prestack migration ellipse (black) produces by NMO, DMO, and migration with a velocity that is 30 percent too low. INMO with the incorrect velocity produces a spread of data, as illustrated by the black curve in Figure 7c. At this point, more accurate velocities can be estimated. If the exact velocity is applied, the output is the black curve in Figure 7d. Note the comparison with the correct shape shown in gray. The steeper dips that should be contained in the black curve have been misspositioned.

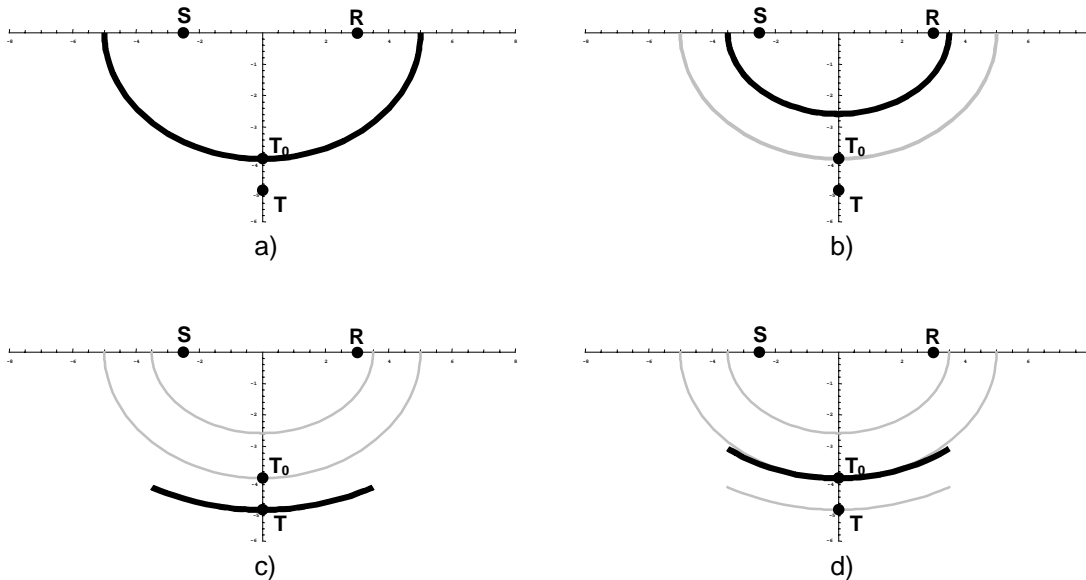


Figure 7 Sequence illustrating a) the correct prestack migration ellipse, b) the ellipse that results with incorrect velocities, c) the result of INMO, and d) the application of the correct NMO to the image in (c).

This method requires the entire DMO and migration loop to be repeated after a new velocity has been selected, and may require a number of iterations to converge to the correct velocities.

The ideal application of NMO, DMO, poststack migration, and INMO on constant offset sections will reconstruct data from Cheop's pyramid to a hyperbola on the gather at the CMP location (possibly referred to as CRP or CDP). The elimination of INMO produces a constant time event across the offset planes that can be stacked at the scatterpoint location.

As in the previous section, care must be taken when using stacking velocities as the initial guess. The effects of dipping events on the stacking velocities should be removed.

The results using NMO-DMO-poststack migration:

- Problem of conflicting dips is eliminated.
- Iterative solutions are required.
- Two separate velocity functions required: NMO and poststack migration.

Gardner's DMO

A method that applies DMO before NMO (Forel and Gardner, 1988) is referred to as Gardner's DMO or GDMO. The process starts with the identical algorithm of the constant offset method, but then modifies the offsets of the traces in the DMO aperture. The results are illustrated in Figure 8, which shows a conventional DMO in (a), and GDMO in (b). In (b) the GDMO'd traces form around a vertical circular cylinder with the DMO ellipse lying on radial planes.

GDMO will convert the Cheop's pyramid (shown again in Figure 9a) to the hyperboloid in Figure 9b where the moveout is hyperbolic in all CMP gathers. NMO applied to the hyperboloid will form the hyperbolic cylinder illustrated in Figure 5b.

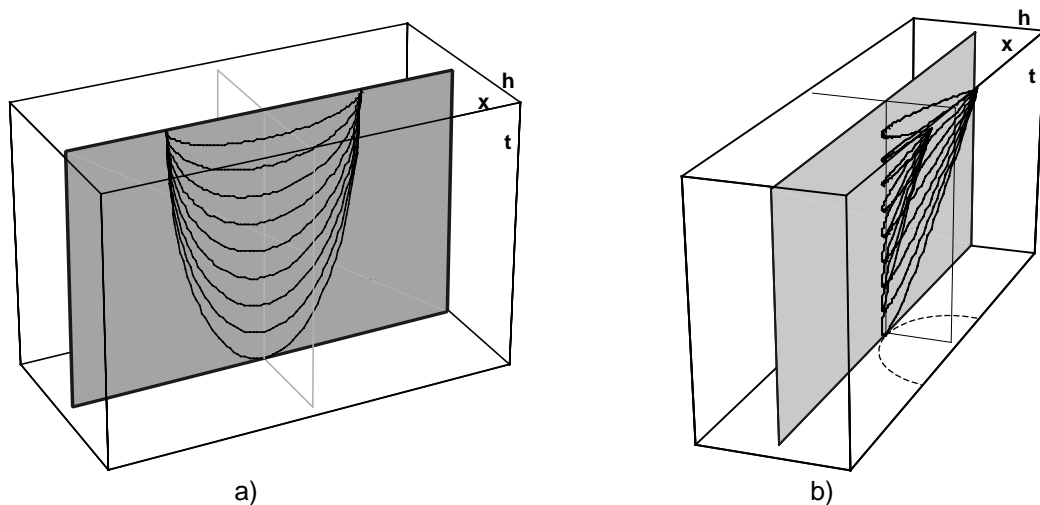


Figure 8 DMO by a) the conventional constant offset method, and b) Gardner's method

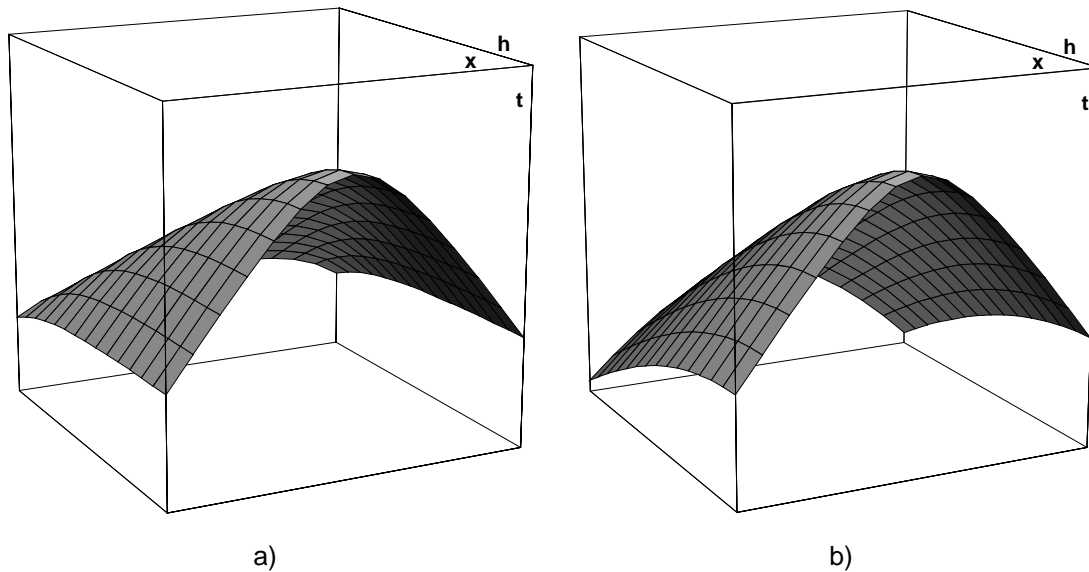


Figure 9 Cheop's pyramid in a) is converted to the hyperboloid in b) by Gardner's DMO.

In a constant velocity environment, all data will be hyperbolic in the CMP gathers and allow the evaluation of this velocity. When extended to variable velocities, the problem of conflicting velocities from different dips still remains. This remaining problem may be visualized by examining the CMP gathers of the hyperboloid in Figure 9b. The velocity for each CMP hyperbola is defined at the apex, however the zero offset times of the CMP gathers increase as they move away from the apex and into areas with different velocities.

GDMO is velocity independent and requires no iterations of the velocity analysis. This property forms the foundation for the DMO-PSI method that follows.

The results using Gardner's DMO:

- Stacking velocities are independent of dip.
- Multiple velocity solutions will remain in areas of conflicting dip.
- Velocities are estimated directly (without iterative solutions).
- Two separate velocity functions required: NMO and poststack migration.

DMO-PSI

DMO (or GDMO)

The previous methods of processing require some form of iterative solution or have problems with conflicting dips. All these deficiencies are eliminated with a process referred to as DMO-PSI.

DMO-PSI is a combination of processes that form prestack migration gathers. These gathers are similar in form to CMP gathers as they are located in similar

positions and contain traces at various offsets. However, a prestack migration gather is formed from all traces in the migration aperture. Another major difference is that energy in the prestack migration gather is positioned at the correct offset for velocity analysis, in contrast to the CMP gather which has the energy positioned at the half source-receiver offset.

Analysis of these gathers yields prestack migration velocities that combine the two separate velocities previously required by NMO and poststack migration. The prestack migration is then achieved by scaling, filtering, applying NMO with the prestack migration velocities, and stacking: we refer to this process as Kirchhoff NMO.

All reflectors may be considered to be composed of scatterpoints that produce corresponding Cheop's pyramids in the prestack volume. The DMO part of the process is Gardner's DMO that reconstructs the data from the Cheop's pyramids into hyperboloids. At this point, the hyperboloids overlap each other and limit velocity analysis. The next step in the process, PSI (prestack imaging), removes the problem of overlapping reflections.

Prestack Imaging (PSI)

Consider any vertical plane through the scatterpoint or apex of one hyperboloid: the scattered energy will lie on the same hyperbola. The summation of the energy from all these planes will also be hyperbolic, and may be summed into a single gather at the scatterpoint location. We refer to this prestack migration gather as a common scatterpoint (CSP) gather as it contains a reinforcement of the scattered energy. If another CSP gather is formed at a new CMP location a few traces to one side of the scatterpoint, the energy from the hyperboloid will be disbursed on the CSP gather. Kirchhoff NMO of the two CSP gathers will result in a concentration of energy at the scatterpoint, and cancellation at all other locations.

PSI is just a process that rotates energy into a CSP gather, and may be visualized from a time slice ($x, h, t = t_a$) through the prestack volume as shown in Figure 10a. The slice through each hyperboloid will produce a semicircle with the center at the CSP location. A modelling program (inverse of migration) would collapse the energy of these semicircles to a point adjacent to the CSP location as illustrated in Figure 10b. Modelling of all time layers would reconstruct the energy from Cheop's pyramid to a hyperbola on the CSP gather as illustrated in the images of Figure 11. The reconstruction is independent of any velocity and is suitable for any velocity structure.

DMO-PSI may implemented using a number of different Fourier transform domains. The DMO portion may be accomplished one trace at a time in the (x, h, ω) domain where the DMO is accomplished by the Liner method (Liner 1990) then shifted to the new offsets h_{DMO} . Additional transforms to the (K_x, K_{h-DMO}, ω) domain allows for fast PSI (similar to FK modelling). Inverse transforms back to the (x, h_{CSP}, t) domain yield the CSP gathers.

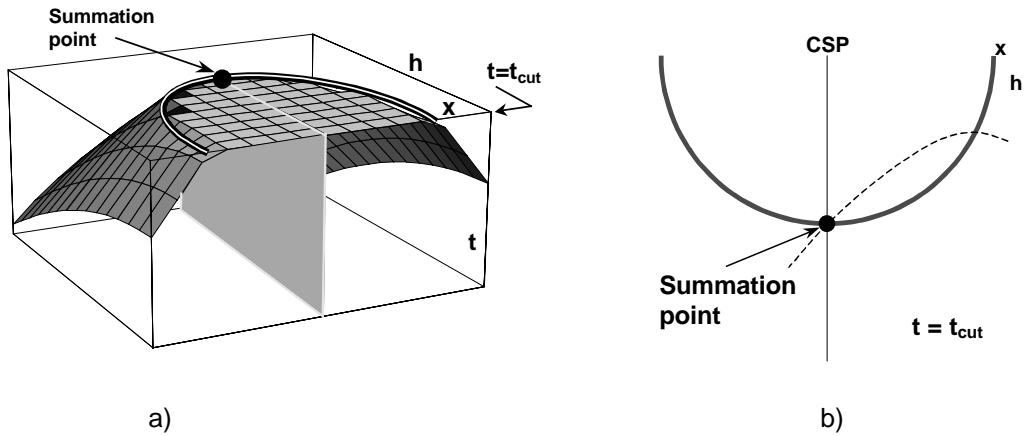


Figure 10 A time-slice of an hyperboloid in a) the prestack volume and b) the corresponding time slice displayed to modelling. Energy on the semicircle will rotate (reconstruct) at the summation point.

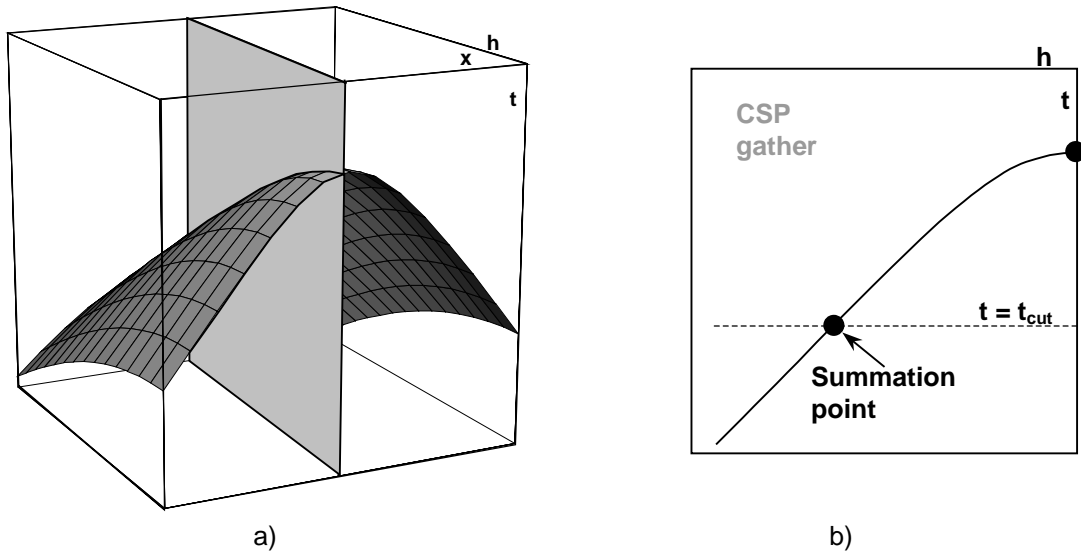


Figure 11 The CSP gather located at the scatter point in a) the hyperboloid, and b) with the energy from the hyperboloid rotated to the CSP hyperbola.

Kinematics of *one* input sample

The kinematic movement of one input sample is illustrated in Figure 12. The sample is GDMO'd, distributed to neighbouring CSP gathers, and then Kirchhoff NMO'd to the prestack migration ellipse. Figure 12a shows the result after GDMO whit energy lying on an ellipse in the radial plane. The kinematics of moving the radial ellipse to the CSP gather is visualized in the rear view of the prestack volume of Figure 12b. This figure shows the energy of the radial ellipse in its initial position, and then after the energy has been mapped to a CSP gather forming a curve referred to as the "DMO-PSI curve".

The DMO-PSI curve is tangent to a scatterpoint hyperbola. Only the energy at the point of tangency contributes to the CSP gather. Energy from many input samples

would reconstruct on the CSP hyperbola and cancel elsewhere to form the desired response.

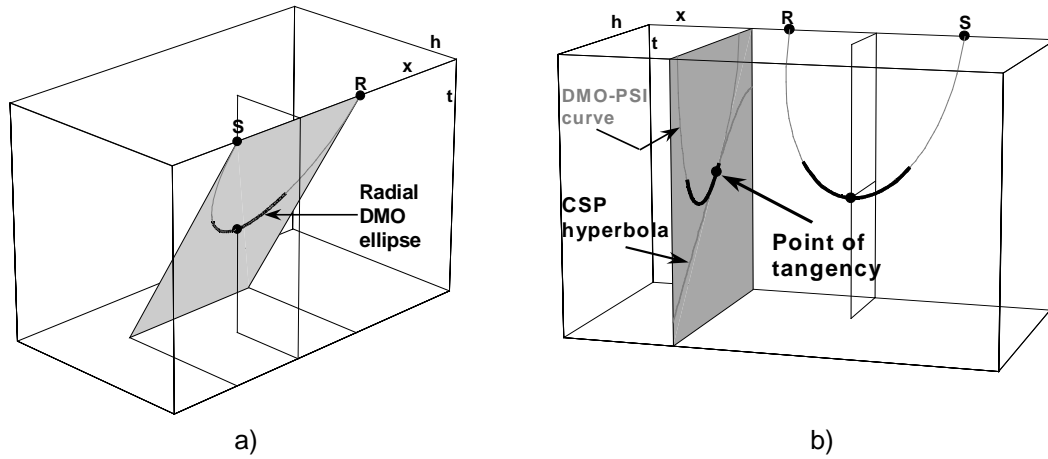


Figure 12 Steps of DMO-PSI showing a) the radial DMO and b) the movement of energy to the CSP gather DMO-PSI curve.

An input sample at T and h can be mapped exactly to the point of tangency (see Appendix2) at a new time T_g and offset h_{psi} given by,

$$T_g^2 = T^2 - \frac{16x^2h^2}{T^2V^4}, \tag{4}$$

$$h_{psi}^2 = x^2 + h^2 - \frac{8x^2h^2}{T^2V_{sp}^2}. \tag{5}$$

A 2-D view of the DMO-PSI curve in a CSP gather is shown in Figure 13. Equations (4) and (5) define the location of the point of tangency.

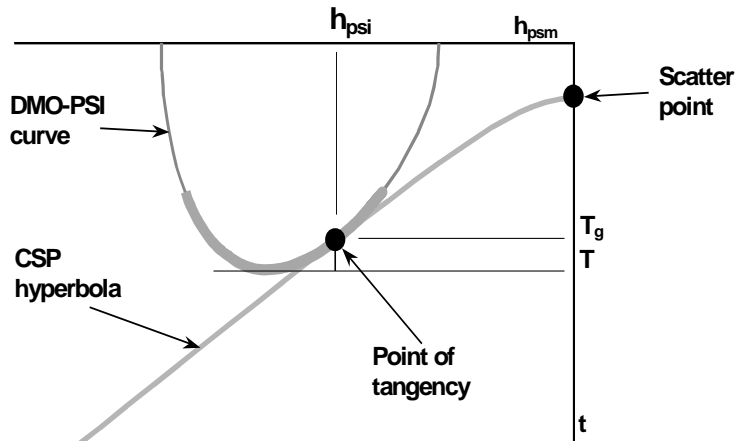


Figure 13 A CSP gather containing DMO-PSI energy from one scatter point. If the input sample came from a scatter point at this location, then the DMO-PSI curve will be tangent to the CSP hyperbola.

It should be emphasized that the mapping of the input sample to the DMO-PSI curve on the CSP gather is independent of velocity. The CSP hyperbolas are velocity dependent, and will all be tangential to the DMO-PSI curve at points that depend on velocity. It is the point of tangency, defined by equations (4) and (5), that varies with velocity.

The mapping of the input sample curve to all CSP gathers is shown in Figure 14. Figure 14a shows the kinematic location of the point of tangency for a given velocity. Figure 14b shows how the application of Kirchhoff NMO moves the point of tangency to the prestack migration ellipse. Figure 14c shows the actual mapping of the input sample to neighbouring CSP gathers. The mapping of this energy with Kirchhoff NMO to reconstruct the prestack migration ellipse is left to the imagination of the reader. Note that the extent of the point of tangency is limited by the boundary of the prestack migration ellipse.

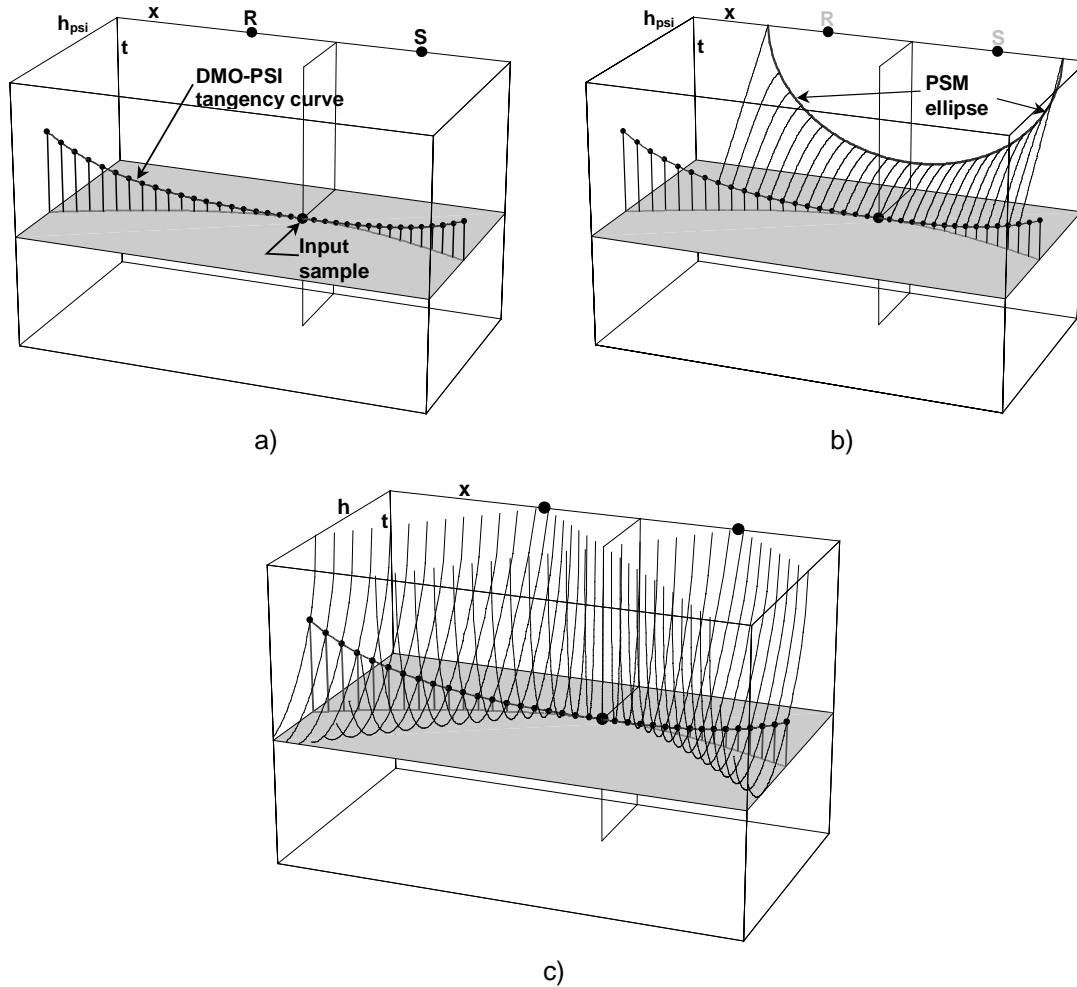


Figure 14. DMO-PSI with a) shows the kinematic location of the point of tangency, b) construction of the prestack migration ellipse using the point of tangency and Kirchhoff NMO, and c) the actual mapping of the input sample to the CSP gathers.

In summary, a one to many mapping of the input sample creates the radial DMO ellipse, and the one to one mapping of PSI moves samples from the radial ellipse to the CSP gather. The desired energy is tangent to the hyperbola on the CSP gather. In comparison, it will be shown that EOM maps the input sample with a one to one mapping of the input sample *directly* to the hyperbola on the CSP gather.

The results using DMO-PSI

- Stacking velocities are independent of dip.
- Conflicting dips have been resolved.
- Velocities are estimated directly (without iterative solutions).
- Only one velocity function (x, t) is required.
- Practical implementations require an even acquisition geometry.

EQUIVALENT OFFSET MIGRATION (EOM)

Definition of the equivalent offset

Equivalent offset migration (EOM) produces similar results to DMO-PSI as both produce CSP gathers (Bancroft and Geiger 1994). However, the method of producing those gathers is significantly different. The EOM method moves an input sample with one-to-one mapping directly to the CSP gather. There is no time shifting and no DMO.

The method computes the location of a co-located source and receiver that maintains the same traveltimes to a scatterpoint as the original source and receiver, as illustrated in Figure 15a and b.

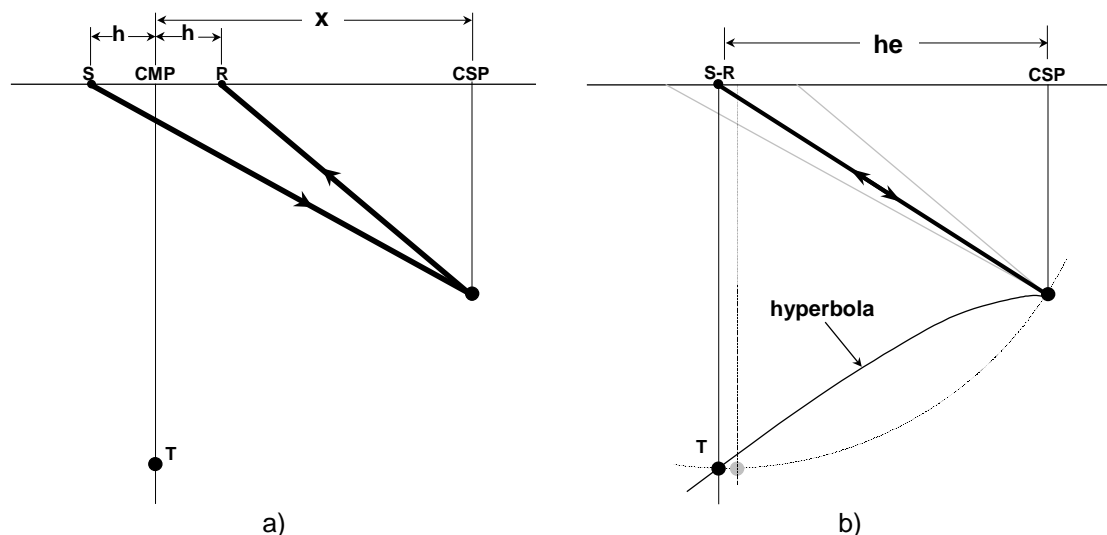


Figure 15 Comparison of a) the actual ray paths, and b) the equivalent offset raypaths with co-located source and receiver.

The offset from the CSP to the co-located source and receiver is defined as the equivalent offset h_e . In essence, the equivalent offset allows the double square root equation to be expressed as to a hyperbola, i.e.,

$$T = \left(T_0^2 + \frac{(x+h)^2}{V^2} \right)^{1/2} + \left(T_0^2 + \frac{(x-h)^2}{V^2} \right)^{1/2} = 2 \left(T_0^2 + \frac{h_e^2}{V^2} \right)^{1/2} \quad (6)$$

where T_0 is the vertical one-way time from the scatterpoint to the surface, V the velocity, x the distance from the CSP to the CMP, and h the half offset. The equivalent offset term h_e may be solved exactly to give;

$$h_e^2 = x^2 + h^2 - \frac{4x^2h^2}{T^2V_{sp}^2} \quad (7)$$

The equivalent offset is both time and velocity dependent as defined by the cross term in equation (7). An input trace (which has constant x and h) will span a range offsets, or cover a range of offset bins in the CSP gather. The first offset h_{e-init} is defined by

$$h_{e-init} = x. \quad (5)$$

The curve defined by h_e has an asymptote at h_{e-asym} as T becomes large and is defined by;

$$h_{e-as}^2 = x^2 + h^2 \quad (6)$$

The previous discussion suggests that h_e must be computed for each input sample. This is not the case. Only the transition times at which the input samples move to a new bin are computed. In addition, the starting point defined by equation (5) represents a ninety degree migration. Restricting the migration dip will also reduce the number of bins spanned by the input trace, further reducing the number of h_e computations.

At a constant time T , the double square-root portion of equation (6) defines a slice through Cheop's pyramid in (x, h) space, while the final term defines a single offset h_e , as illustrated in Figure 16. All points on the Cheop's slice have the same equivalent offset and will sum to the point at h_e on the CSP gather (Figure 16b). All points on the 3-D surface of Cheop's pyramid (x, h, T) will therefore map to the hyperbola on the CSP gather (h_e, T) , as illustrated in Figure 17.

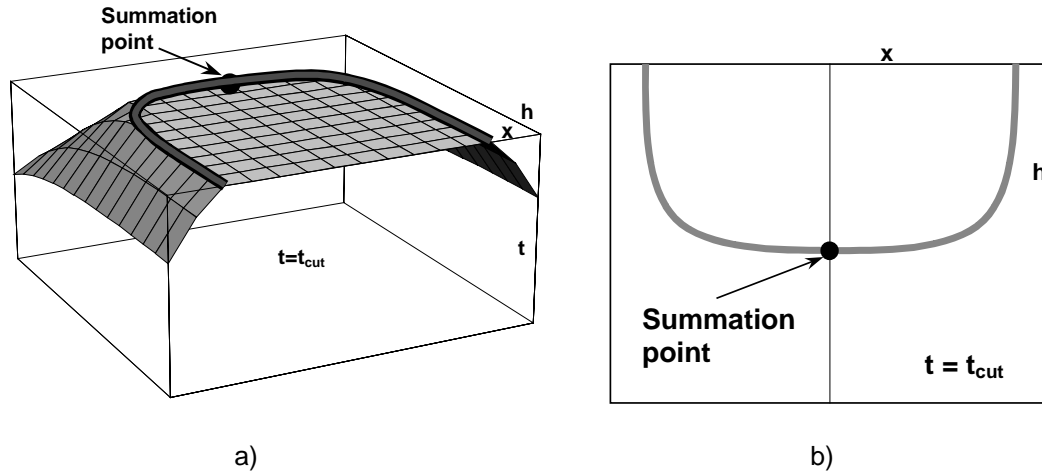


Figure 16. EOM at a constant time T showing a) a time section through Cheop's pyramid, and b) the resulting summation of energy to the CSP gather.

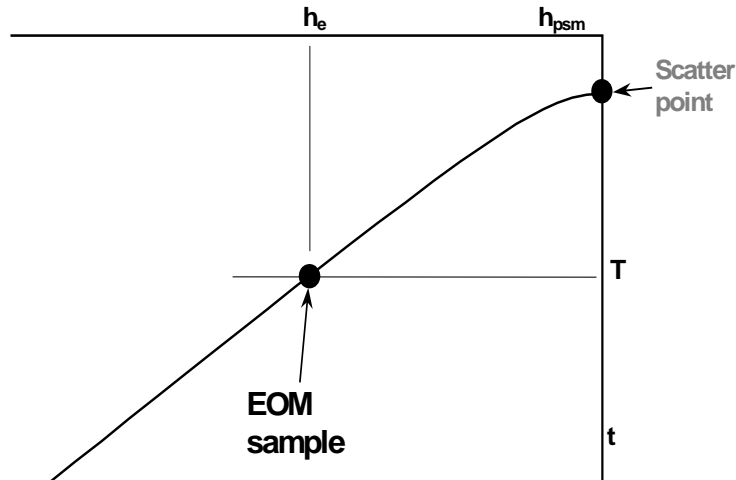


Figure 17. CSP gather showing the location of the input energy and the scatterpoint hyperbola.

Kinematics of EOM for *one* input sample

The previous discussion viewed EOM from a scatterpoint perspective with many input samples spread over Cheop's pyramid. We now consider the distribution approach where we consider the energy movement from one input sample. To accomplish this, we consider equation (4) at a constant time T, offset h, and velocity V. The x variable now represents the displacement from the input CMP location (also constant at $x = 0$) to any CSP gather at x. Equation (4) may now be written as

$$h_e^2 = x^2 \left(1 - \frac{4h^2}{T^2V^2} \right) + h^2. \quad (7)$$

With constant velocity, the term in brackets can be replaced by a constant c, giving

$$h_e^2 - x^2 c = h^2 . \quad (8)$$

Equation (8) is a hyperbola on a plane (x, h_e) at constant T , as illustrated in Figure 18a. Kirchhoff NMO applied to this equivalent offset hyperbola will now form the prestack migration ellipse as illustrated in Figure 18b. Again note that the prestack migration ellipse limits the extent of the energy in the equivalent offset hyperbola.

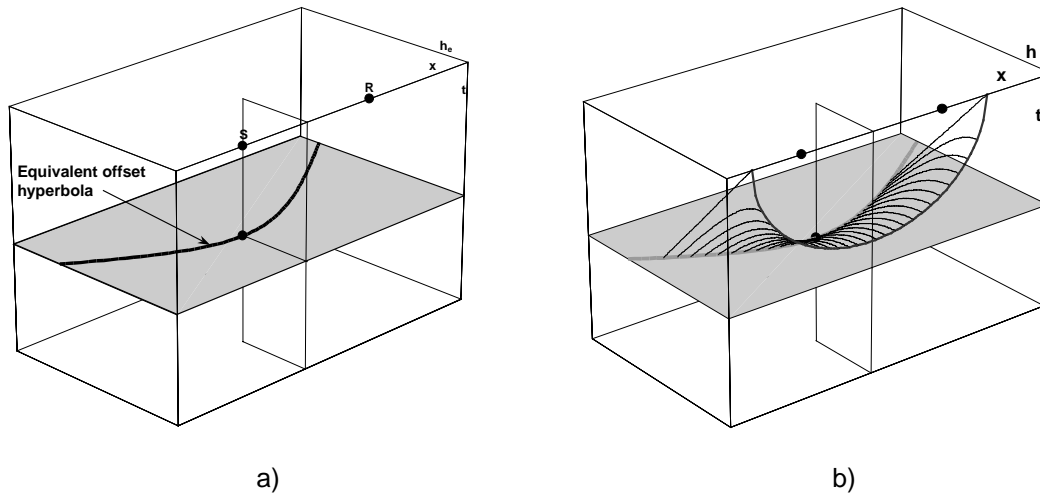


Figure 18 Prestack view of a) the equivalent offset hyperbola at constant time and b), forming the prestack migration ellipse with Kirchhoff NMO.

The results using EOM

- Stacking velocities are independent of dip.
- Conflicting dips have been resolved.
- Insensitive to velocities. (Bancroft and Geiger 1996)
- Only one velocity function is required.
- CSP gathers may be formed at arbitrary locations.
- Fast.

Additional applications permitted by the time domain approach

- Extended to converted wave processing (P-S). (Bancroft and Wang 1994)
- Migrate from rugged surfaces. (Geiger and Bancroft 1996)
- Suitable for uneven acquisition geometries.
- Allows 2-D lines to be prestack migrated from a 3-D project.
- Allows different input geometries to be combined with arbitrary output geometries.
- Used to provide model trace for statics analysis, independent of velocity (Li and Bancroft 1996).

KINEMATIC COMPARISON BETWEEN DMO-PSI AND EOM

The kinematics of DMO-PSI and EOM can be compared using the equations that define the mapping of energy to the CSP gather. For a given velocity V , the point of tangency between the DMO-PSI curve and the hyperbola is at time T_g and offset h_{psi} . The EOM point is defined at the same time as the input T , and at the equivalent offset h_e . The relevant equations are given in Table 1.

Table 1. Comparison of point of DMO-PSI point of tangency with EOM point on a CSP gather.

	Time	Offset
DMO-PSI point of tangency	$T_g^2 = T^2 - \frac{16x^2h^2}{T^2V^4}$	$h_{psi}^2 = x^2 + h^2 - \frac{8x^2h^2}{T^2V_{sp}^2}$
EOM	T (no time shift)	$h_e^2 = x^2 + h^2 - \frac{4x^2h^2}{T^2V_{sp}^2}$

The DMO-PSI curve and point of tangency is compared with the EOM point in Figure 19. Note the EOM point is even with the bottom of the DMO-PSI curve. Both the point of tangency and EOM point lie on the scatterpoint hyperbola.

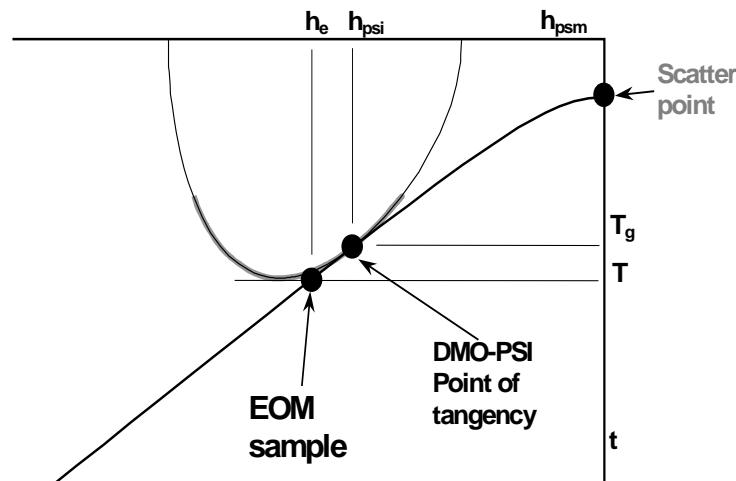


Figure 19. A CSP gather comparing the kinematics of DMO-PSI and EOM.

Figure 20a shows a comparison between the DMO-PSI point of tangency and the EOM point in the prestack volume. Note the EOM point remains on the plane defined by the input time while the DMO-PSI point of tangency is shifted in both offset and time. Part (b) of this figure includes the Kirchhoff NMO hyperbola that maps both sets of points to the prestack migration ellipse. A more accurate comparison is between the full DMO-PSI curves in Figure 14c, with the simple EOM hyperbola in Figure 18a.

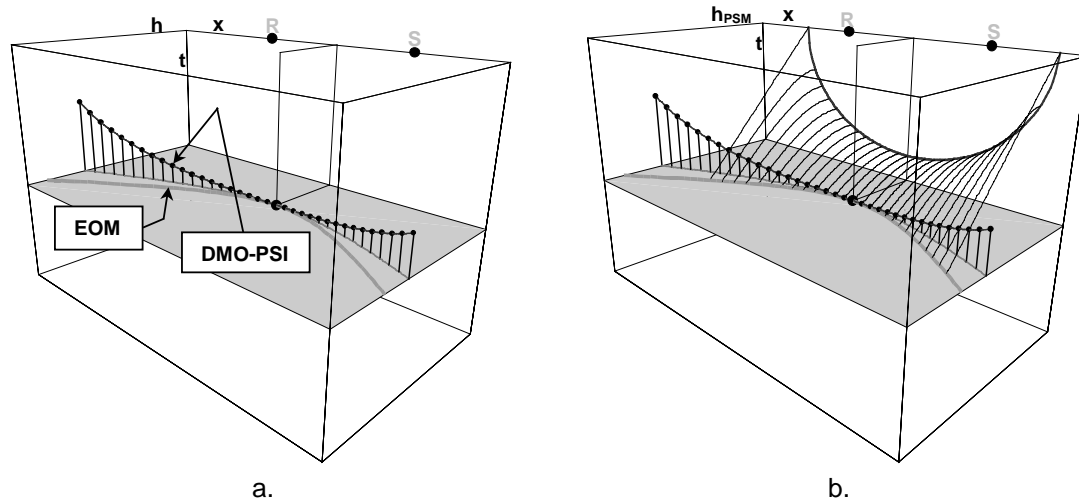


Figure 20 Comparison of a) DMO-PSI with EOM at various SCP locations, and b) with Kirchhoff NMO added to illustrate both methods move energy to the prestack migration ellipse.

An alternate view of the two processes may be gained by studying the images in Figure 21. The impulse response of EOM is kinematically identical to that of constant offset prestack migration. In Figure 21a, an impulse at (x_o, h_o, t_o) is first mapped to a hyperbola (I) in the $t = t_o$ plane of (x, h_e, t) space. This hyperbola is $h_e(x)$ defined by setting h and t to constants in equation (7) and is the contribution of the impulse to the family of CSP gathers. Then each point on the hyperbola is summed along a hyperbolic NMO trajectory in offset and time (II) defined by equation (6). The family of NMO hyperbolae forms the correct prestack migration ellipse (III) where they intersect the zero offset plane. Though this might seem complex at first, it leads to great computational savings because the formation of CSP gathers allows a convenient binning (in h_e), the gathers are formed by trace mappings at constant time, and imaging operations are performed only on the CSP gathers.

In Figure 4b, 4c, and 4d the formation of a single output point of Figure 21a is shown in three different 2-D perspectives for comparison of EOM-NMO, GDMO-PSI-NMO, GDMO-NMO-post stack migration, NMO-DMO-post stack migration, and NMO-prestack migration. (We do not give the numerical details for algorithms other than EOM here because they are well documented in the references.) The distinction between DMO-PSI and EOM is clear in that the GDMO step in the former shifts energy in all three coordinate directions prior to the constant-time PSI process. Furthermore, the hyperbolic constant-time trajectories of PSI and EOM are mathematically distinct as is expected since the latter is collapsing a more complex surface (i.e. Cheop's pyramid). The EOM mapping is computationally simple and efficient (Bancroft et. al., 1997) and the avoidance of the GDMO step is a significant advantage. In particular, EOM is a more flexible algorithm, easily adapted to handle such problems as irregular recording geometry, topographic corrections, residual statics estimation, and converted wave (P-SV) imaging.

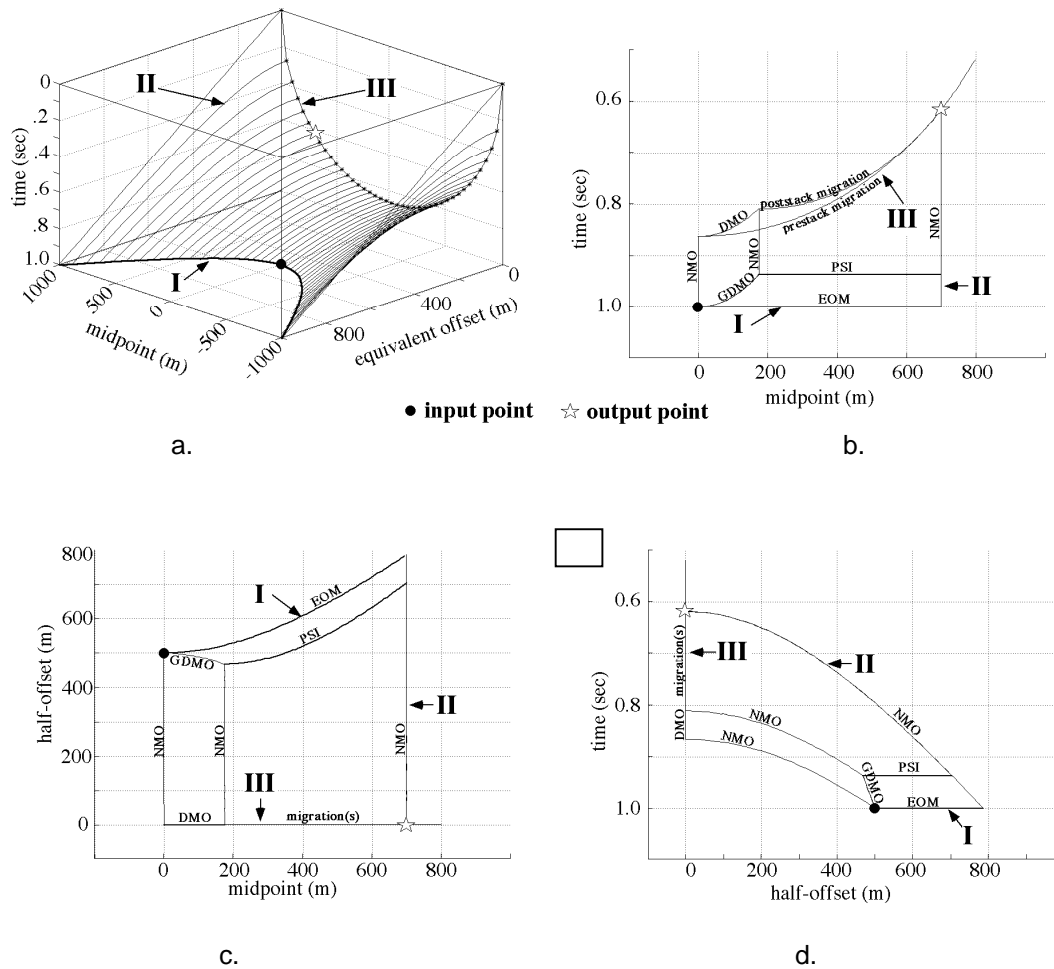


Figure 21. A kinematic comparison of DMO-PSI and EOM from three orthogonal axis.

COMMENTS

A recent paper by Fowler (1997) also compared the kinematics of DMO-PSI, EOM, and other prestack migrations that collapse energy on Cheop's pyramid to CSP gathers. He produced a general travel time equation from which many methods may be used to accomplish similar tasks. When making his DMO-PSI comparison, only the direct mapping of the point of tangency was used, and the DMO portion of the exercise bypassed.

CONCLUSIONS

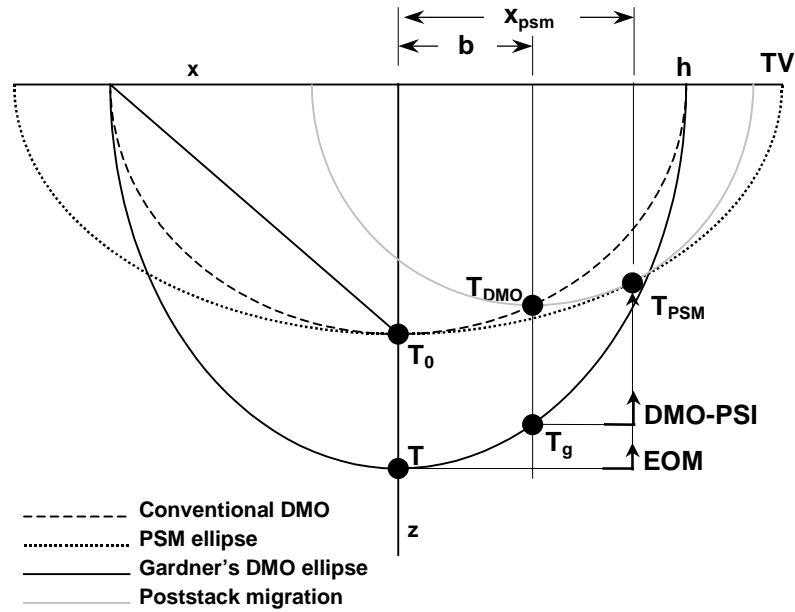
DMO-PSI is kinematically different from EOM.

REFERENCES

References

- Bancroft, J. C., and Geiger, H. D., 1996, Velocity sensitivity for equivalent offset prestack migration: a contrast in robustness and fragility: Expanded Abstracts 1996 CSEG Convention.
- Bancroft, J. C., and Geiger, H. D., 1994, Equivalent offsets and CRP gathers for prestack migration, Expanded Abstracts 1994 SEG International Convention, pp. 672-675.
- Bancroft, J. C., Geiger, H. D., Foltinek, D. S., and Wang, S., 1994 Prestack migration by equivalent offsets and CSP gathers, CREWES 1994 Research Report.
- Bancroft, J. C., and Wang, S., 1994, Converted-wave prestack migration and velocity analysis by equivalent offsets and CSP gathers, CREWES 1994 Research Report.
- Bancroft, J. C., Wang, S., Foltinek, D. S., and Geiger, H. D., 1995 Common scatterpoint (CSP) prestack migration, 1995, Expanded Abstracts CSEG 1995 National Convention.
- Dix, C. H., 1955, Seismic velocities from surface, *Geophysics*, 20, 86-86.
- Forel D. and Gardner, G., 1988, A Three-Dimensional Perspective on Two-Dimensional Dip Moveout, *Geophysics*, 53, 604-610.
- Geiger, H., Bancroft, J. C., 1996, Equivalent offset prestack migration - application to rugged topography and formation of unmigrated zero offset section, EAGE 58th Conference Extended Abstracts, P098.
- Li, X., and Bancroft, J. C., 1996, Surface consistent statics correction associated with EOM, CREWES 1996 Research Report.
- Liner, C. L., 1990 General theory and comparative anatomy of dip moveout, *Geophysics*, Vol. 55, p. 595-607.
- Taner, M. and Koehler, F., 1969, Velocity Spectra-Digital Computer Derivation and Applications of Velocity Functions, *Geophysics*, 34, 859-881.

Appendix 1 Derivation of the tangential location on the DMO-PSI curve



Defined values: T, V, T_0, x_{PSM} ,

Computed values: b, T_{DMO}, T_{PSM}, T_g ,

All time are shown in the Figure as one-way times, however they are computed as two-way times

The equation of the prestack migration (PSM) ellipse is:

$$\frac{4x^2}{T^2V^2} + \frac{4z^2}{T_0^2V^2} = 1. \tag{A1}$$

The equation for poststack migration semicircle is:

$$(x - b)^2 + z^2 = \frac{V^2T_{DMO}^2}{4}. \tag{A2}$$

The equation for the DMO ellipse is:

$$\frac{x^2}{h^2} + \frac{4z^2}{T_0^2V^2} = 1 \tag{A3}$$

The equation for the Gardner's DMO ellipse is:

$$\frac{x^2}{h^2} + \frac{4z^2}{T^2V^2} = 1 \quad (\text{A4})$$

The normal moveout corrected time T_0 is found from;

$$T_0^2 = T^2 - \frac{4h^2}{V^2}. \quad (\text{A5})$$

The value for b is the center of the poststack migration semicircle that is tangent to the PSM ellipse. At this point the slopes or derivatives are equal. The slope on the PSM ellipse is found from,

$$\frac{8x}{T^2V^2} + \frac{8z}{T_0^2V^2} \frac{dz}{dx} = 0 \quad (\text{A6})$$

or,

$$\frac{dz}{dx} = -\frac{x T_0^2}{z T^2} \quad (\text{A7})$$

and the slope on the circle is found from,

$$2(x - b) + 2z \frac{dz}{dx} = 0, \quad (\text{A8})$$

or

$$\frac{dz}{dx} = -\frac{x - b}{z}. \quad (\text{A9})$$

Equating the slopes we get;

$$\frac{x T_0^2}{T^2} = x - b \quad (\text{A10})$$

and solving for b ,

$$b = x - \frac{x T_0^2}{T^2} \quad (\text{A11})$$

$$b = x - \frac{x \left(T^2 - \frac{4h^2}{V^2} \right)}{T^2} \quad (\text{A12})$$

giving,

$$b = \frac{4xh^2}{T^2V^2} \quad (\text{A13})$$

Solving Gardner's DMO ellipse for z we get;

$$z^2 = \frac{T^2V^2}{4} \left(1 - \frac{x^2}{h^2} \right). \quad (\text{A14})$$

Therefore solving at $x = b$, we find T_g from;

$$T_g^2 = \frac{4z^2}{V^2} = T^2 \left(1 - \frac{b^2}{h^2} \right) \quad (\text{A15})$$

$$T_g^2 = T^2 - \frac{T^2b^2}{h^2}. \quad (\text{A16})$$

$$T_g^2 = T^2 - \frac{T^2}{h^2} \left(\frac{4xh^2}{T^2V^2} \right)^2. \quad (\text{A17})$$

$$\boxed{T_g^2 = T^2 - \frac{16x^2h^2}{T^2V^4}}. \quad (\text{A18})$$

The sample at T_g is shifted to a new offset k defined by

$$k^2 = h^2 - b^2. \quad (\text{A19})$$

PSI will then rotate the sample from the DMO'd position to the offset h_{psi} on the CSP gather located at x_{psm} , i.e.,

$$h_{psi}^2 = k^2 + (x - b)^2. \quad (\text{A20})$$

or

$$h_{psi}^2 = h^2 - b^2 + x^2 + b^2 - 2xb. \quad (\text{A21})$$

Substituting b , we get

$$h_{psi}^2 = h^2 - b^2 + x^2 + b^2 - 2x \left(\frac{4xh^2}{T^2V^2} \right). \quad (\text{A22})$$

or

$$h_{psi}^2 = h^2 + x^2 - \frac{8x^2h^2}{T^2V^2}. \quad (A23)$$

The kinematics of Kirchhoff NMO for DMO-PSI is;

$$T_g^2 = T_{PSM}^2 + \frac{4h_{psi}^2}{V^2}. \quad (A24)$$